Cost-Effective Condition Monitoring for Wind Turbines

Wenxian Yang, Peter J. Tavner, *Senior Member, IEEE*, Christopher J. Crabtree, and Michael Wilkinson

***Abstract*—Cost-effective wind turbine (WT) condition monitoring assumes more importance as turbine sizes increase and they are placed in more remote locations, for example, offshore. Conventional condition monitoring techniques, such as vibration, lubrication oil, and generator current signal analysis, require the deployment of a variety of sensors and computationally intensive analysis techniques. This paper describes a WT condition monitoring technique that uses the generator output power and rotational speed to derive a fault detection signal. The detection algorithm uses a continuous-wavelet-transform-based adaptive filter to track the energy in the prescribed time-varying fault-related frequency bands in the power signal. The central frequency of the filter is controlled by the generator speed, and the filter bandwidth is adapted to the speed fluctuation. Using this technique, fault features can be extracted, with low calculation times, from direct- or indirect-drive fixed- or variable-speed WTs. The proposed technique has been validated experimentally on a WT drive train test rig. A synchronous or induction generator was successively installed on the test rig, and both mechanical and electrical fault-like perturbations were successfully detected when applied to the test rig.**

***Index Terms*—Adaptive signal processing, condition monitoring, fault diagnosis, induction generators, signal processing, synchronous generators, time–frequency analysis, wavelet transforms, wind power generation.**

NOMENCLATURE

A	Estimated energy of the frequency component of interest.
$a_{\min}$, $a_{\max}$	Minimum and maximum wavelet scales considered by the adaptive bandpass filter.
a	Wavelet scale.
b	Wavelet time-shift parameter.
ε	Voltage or current transducer error.
e	Specific unbalance.
f_{rm}	Rotational frequency of the generator rotor.
f_{se}	Electrical supply frequency.
G	Balance quality grade.
I_i	Line currents.
m	Unbalanced mass.
$M_{\rm eq}$	Equivalent mass of the test rig rotor.
ω	Angular frequency of interest.
ω_c	Mean frequency of the prescribed frequency component during the time interval T.
$\omega_{\rm fg}$	Fluctuation of the generator rotational frequency.
ω_f	Fluctuation of the frequency of interest.
$\omega_{\rm upper}$, $\omega_{\rm lower}$	Upper and lower cutoff frequencies of the adaptive filter.
ω_0	Central angular frequency of the mother wavelet.
ω_{rm}	Angular rotational frequency of the generator rotor.
P	Three-phase total power output from the generator.
r	Effective radius of the equivalent unbalanced mass.
R_{AB}, R_{BC}, R_{CA}	Combined line-to-line resistances.
R_{AS}, R_{BS}, R_{CS}	Brush gear and slip ring resistances.
R_{AV}, R_{BV}, R_{CV}	Load bank resistances.
R_A, R_B, R_C	Generator rotor winding resistances.
δR	Electrical resistance imbalance.
s	Induction machine slip.
ψ	Mother wavelet function.
T	Sliding window averaging time interval.
t_0	Starting time moment of the sliding window.
U_e	Electrical asymmetry on the generator rotor.
U_m	Mechanical unbalance on the generator rotor.
V_i	Phase voltages.
x	Real-time signal.
η	Constant between $\omega_{\rm fg}$ and ω_f.

Manuscript received December 5, 2008; revised September 3, 2009. First published September 22, 2009; current version published December 11, 2009. This work was supported by the U.K. Engineering and Physical Sciences Research Council Supergen Wind Program EP/D034566/1.

W. Yang is with the New and Renewable Energy Centre, NE24 3AG Blyth, U.K.

P. J. Tavner is with the School of Engineering and Computing Sciences, Durham University, DH1 3LE Durham, U.K. (e-mail: Peter.Tavner@durham.ac.uk).

C. J. Crabtree is with Durham University, DH1 3LE Durham, U.K.

M. Wilkinson is with Garrad Hassan, BS2 0QD Bristol, U.K.

Color versions of one or more of the figures in this paper are available online at http://ieeexplore.ieee.org.

Digital Object Identifier 10.1109/TIE.2009.2032202

I. INTRODUCTION

OVER THE last 40 years, there has been an increased application of wind turbines (WTs) around the world, with growth in rating from 30 kW to $>$ 5 MW and, more recently, their application offshore [1]. To reduce the cost of energy from WTs, there is a pressing need to improve the WT availability and reduce the operational and maintenance (O&M)

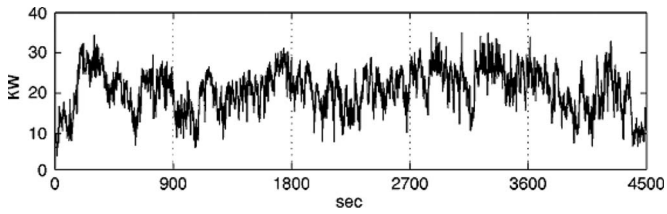

Fig. 1. Variation in power output from a 33-kW fixed-speed WT over five successive periods of 900 s, each showing the large variation in the signal due to wind turbulence (taken from [7]).

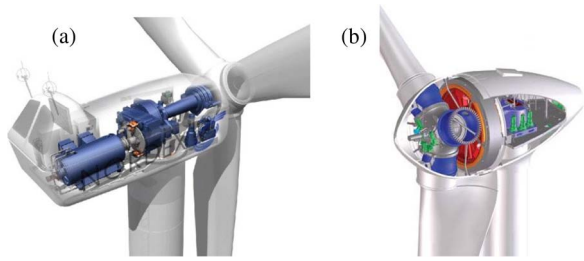

Fig. 2. Structures of real large WTs. (a) Geared. (b) Direct drive.

costs. Aside from developing more advanced machine designs [2] to improve the availability, an effective way to achieve this improvement would be to apply reliable and cost-effective condition monitoring [3], which is why this subject is attracting industrial and academic attention.

The wind industry currently uses condition monitoring systems (CMSs), such as vibration, temperature, lubrication oil, and generator current analysis, developed from other rotating machine power generation industries [4]–[6], where they have achieved success. However, despite their application in the wind industry [7], they have not yet proven their effectiveness due to the peculiarities of a WT, which has a slow speed and rapidly varying torque. Commercial WT CMSs mostly employ vibration-based techniques, which are sophisticated, and the sensors and cabling are costly. The technique is also not ideally suited to all WT types and faults. Lubrication oil analysis is becoming more popular for detecting gearbox tooth and bearing wear but cannot detect failures outside the gearbox. More advanced techniques, such as optical strain measurement, have been developed for monitoring WT blade integrity. However, these are expensive, and recent reliability surveys [8] have shown that WT electrical systems have a higher failure rate than the mechanical systems. For these reasons, an electrically based WT CMS would be beneficial and could be more comprehensive, simpler, and cheaper than other techniques. This paper will propose such a technique.

Instantaneous electric power measurement has been demonstrated on induction machines for detecting motor faults [9]. Three-phase total power monitoring has also been applied to WTs as a condition monitoring and fault diagnosis signal [10] but has not achieved commercial application. This research will be based entirely on the use of this signal and the generator speed for condition monitoring. Power output measurement was considered for condition monitoring in [7] and [10], but Fig. 1, taken from [7], shows how the WT power output signal experiences continuous and rapid variations during operation.

The work reported in this paper is an enhancement of the research described in [11], now including the following:

1) a more comprehensive description of the background technology and the state of the art of the proposed technique;
2) an improved mathematical presentation;
3) additional figures to enhance the description of the technique;
4) more substantial experimental results;
5) an amended conclusion.

The novelties of the proposed technique are summarized as follows:

1) a technique for WT condition monitoring based on measuring the generator total power signal rather than more conventional measurements validated by experiments on a test rig with a simple fault setup;
2) a new adaptive continuous-wavelet-transform (CWT)-based energy tracking method, reducing the calculation time for feature extraction when applied to lengthy signals, making possible less time-intensive WT condition monitoring;
3) the successful detection of two types of fault using this method has been demonstrated on two WT arrangements, including both electrical and mechanical faults;
4) the proposed method is more efficient for the detection of faults in variable-speed WTs than other more conventional techniques;
5) the technique used in this paper can be applied to any WT generator for tracking any characteristic, fault-related frequency component, so it is general and could be applied to detect a variety of faults depending on the choice of frequency selected.

Wavelet transforms have been successfully used in condition monitoring and diagnosis of rotating electrical machine faults [1], [12]–[14]. However, most used the discrete wavelet transform (DWT) rather than the CWT, although the latter is superior to the former in multiresolution signal analysis. However, the CWT involves more intensive convolution calculations than the DWT, making it more difficult to process lengthy online data, such as WT monitoring signals. Moreover, it is inconvenient to apply the traditional time–frequency–amplitude CWT image to machine condition monitoring, as was done in [15]. Wavelets have been proposed for WT condition monitoring [16], [17] but have not yet received commercial application.

II. Applying Generator Power Monitoring to WTs

A WT converts the kinetic energy of the wind into electrical energy, utilizing mechanical and electrical conversion, control, and transmission systems. The architectures of two commonly used large WTs are shown in Fig. 2.

The application of vibration, temperature, and lubrication oil techniques to monitoring WTs should improve their availability but, to date, is not being widely used for the following reasons:

1) lack of practical industry experience with condition monitoring in the wind environment;
2) difficulties collecting and interpreting the data, including the risk of false or missed alarms;

3) the fact that present techniques may not be suited to all types of WTs such as shown in Fig. 2;
4) the fact that developing reliable WT condition monitoring techniques requires complex and lengthy collaboration between WT operators and manufacturers in the field.

WT power flows are disturbed by both mechanical and electrical faults [16], [17]. To measure the WT shaft torque is costly and usually impractical for a real WT. In contrast, shaft speed and electrical power output are routinely monitored for WTs, but, to date, commercial CMSs do not use these signals.

In comparison with conventional stator current analysis, widely adopted for condition monitoring motors [4], [6], power monitoring could have the following disadvantages.

1) The error in the total power signal depends not only on the voltage and current transducer error ε but also on the measurement method. In the three-wattmeter method, the error will be 6ε, but, in the two-wattmeter method, the error is limited to 4ε, whereas the current signal error would be only ε. Therefore, the signal-to-noise ratio for basic analysis should be better for current than power analysis.

On the other hand, monitoring based on power analysis could have the following advantages.

1) The power signal is already available from the generator terminal voltage and current signals for the control of the WT and can conveniently be accessed.
2) Fewer cheaper transducers than accelerometers and oil debris probes are required for power monitoring.
3) Mechanical and electrical faults both disturb the generator power output, so power monitoring could detect both types of faults.
4) Single line current analysis contains the mains frequency carrier, whereas this is absent in the power signal. Therefore, the signal-to-noise ratio for faulty feature analysis should be better for power than current analysis, balancing the aforementioned transducer error effect.
5) In the power signal, the fault-related frequency sidebands, around the mains frequency, are folded down around dc, limiting the bandwidth needed to monitor the signal.

An example of the current, voltage, and power signals measured under faulty conditions on an induction generator, fitted to the test rig described in the following, is shown in Fig. 3, where the signals were collected when a periodic rotor electrical asymmetry was applied in the presence of serious noise due to power system imbalance.

The fault in Fig. 3 was applied at the time intervals of 20–40 s and 60–80 s and was absent in the other time intervals. It can be seen that the amplitudes of both the current–time and voltage–time waveforms gave no indication of abnormal conditions, whereas the total three-phase power signal P changes significantly during the abnormality due to the presence of $2f_{se}$ and $2sf_{se}$ components. The total power $P(t)$ was calculated using

$$P(t) = \sum_{i=1}^{3} I_i(t) \cdot V_i(t). \tag{1}$$

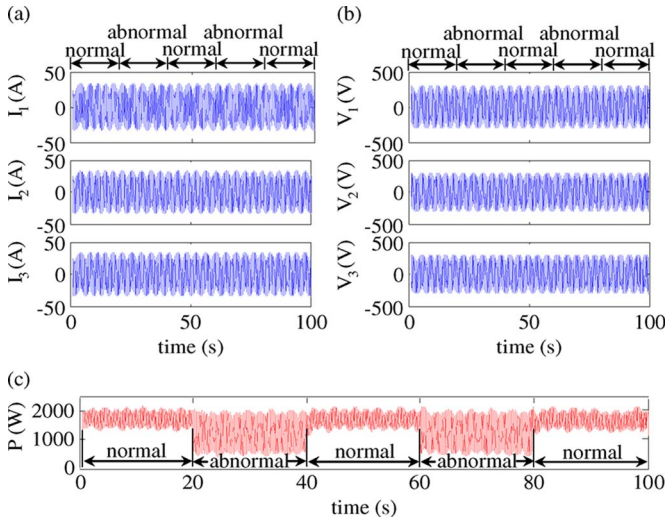

Fig. 3. Comparison of current, voltage, and total power signal in the presence of a rotor asymmetry fault. (a) Line currents. (b) Phase voltages. (c) Total power.

III. Design of Wavelet-Based Adaptive Filter

In this paper, a CWT-based adaptive filter has been designed to track the energy in the power signal in the prescribed fault-related frequency bands rather than at all frequencies of the monitoring signal. In this way, the wavelet calculation can significantly be reduced, and the results can be displayed graphically rather than as a screen dump image, making the technique attractive for online application. Details of the technique are described as follows.

The CWT of a real-time signal $x(t)$ can be defined as

$$\text{CWT}(b,a) = \frac{1}{\sqrt{|a|}} \int_{-\infty}^{\infty} x(t)\psi^* \left(\frac{t-b}{a}\right) dt \tag{2}$$

where the asterisk "$*$" indicates the complex conjugate.

Traditionally, the wavelet function $\psi(t)$ is dilated or compressed by changing the scale parameter a so that all signal components ranging from frequency 0 to half the sampling frequency can be projected onto an appropriate time-scale map, as shown in Fig. 4. The bottom figure shows the time waveform of a sample signal of increasing frequency being inspected; the top figure shows the wavelet coefficients of this signal obtained at different wavelet scales and times.

Many of the calculations shown in Fig. 4 are unnecessary for WT condition monitoring because the fault-related frequencies are few in number and the energy extracted at nonfault-related frequencies is not helpful to assess the machine condition.

Therefore, an adaptive CWT-based filter has been designed, which only extracts energy at known fault frequencies, while frequencies unrelated to the fault are left unprocessed. The calculation time for the new technique will be much shorter than that for a conventional CWT applied to a broad bandwidth signal. Therefore, the proposed CWT-based energy tracking technique should prove more efficient for online processing of WT monitoring signals than conventional CWT processing.

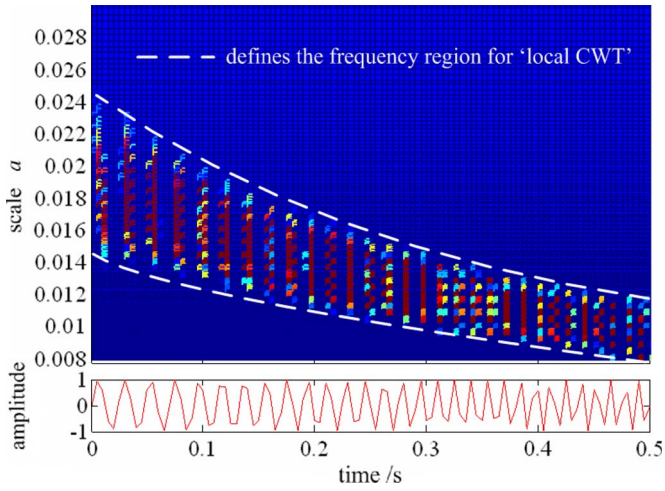

Fig. 4. Illustrative example of the conventional CWT.

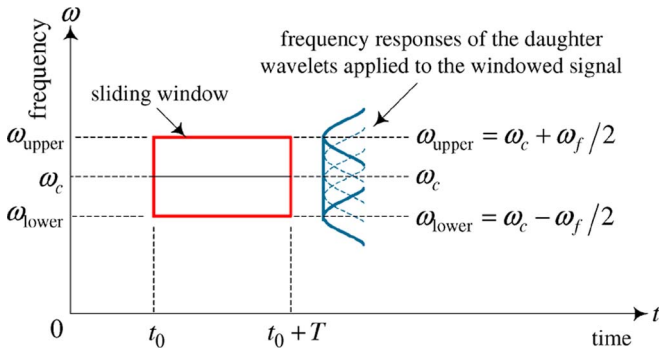

Fig. 5. Two-dimensional sliding window.

A time–frequency sliding window has been designed for this task, as shown in Fig. 5. Its central frequency ω_c is the mean frequency during the time interval T of the prescribed fault-related frequency band. The upper and lower cutoff frequencies ω_{upper} and ω_{lower} are adapted to the fluctuation of the generator rotational speed ω_{fg} in that interval, i.e.,

$$\begin{cases} \omega_{\text{upper}} = \omega_c + \omega_f/2 \\ \omega_{\text{lower}} = \omega_c - \omega_f/2 \\ \omega_f = \eta\omega_{\text{fg}}. \end{cases} \tag{3}$$

From Fig. 4, it is noticed that ω_f could also be a time-varying parameter, intrinsically dependent on the turbulence of the wind. Experience has shown that onshore wind turbulence varies between 12% and 20%, whereas offshore turbulence approximates to ∼6%.

The relationship between any prescribed frequency ω and its corresponding wavelet scale a is

$$a = \frac{\omega_0}{\omega}. \tag{4}$$

With the aid of (3) and (4), the range of the wavelet scales for conducting bandpass filtering can be determined by

$$a \in [a_{\min} \quad a_{\max}] \tag{5}$$

$$\begin{cases} a_{\min} = \frac{\omega_0}{\omega_{\text{upper}}} \\ a_{\max} = \frac{\omega_0}{\omega_{\text{lower}}}. \end{cases} \tag{6}$$

TABLE I
COMPUTATIONAL EFFICIENCY COMPARISON BETWEEN CWT, DWT, AND PROPOSED APPROACH

Method	Time cost	Operation manner	Accuracy
CWT	18.91s	All frequencies between zero and half sampling frequency are calculated.	Good
DWT	0.31s	Interested frequency band is determined in a rigid dyadic step way.	Not good
Energy tracking	0.16s	Interested frequency band is determined intelligently.	As good as CWT

Subsequently, by performing the CWT locally in the scale range defined by (5), a matrix of wavelet coefficients is obtained

$$\text{CWT}_{\text{local}}(b,a) = \frac{1}{\sqrt{|a|}} \int_{-\infty}^{\infty} x(t)\psi^*\left(\frac{t-b}{a}\right) dt. \tag{7}$$

The energy A of the frequency component of interest in the time interval T is estimated by

$$A(t_0 + T/2) = \max\left(|\text{CWT}_{\text{local}}(b,a)|\right) \quad \begin{cases} a \in [a_{\min} \quad a_{\max}] \\ b \in [t_0 \quad t_0 + T]. \end{cases} \tag{8}$$

The sliding window is moved forward along the signal; the maximum and minimum wavelet scales in (5) being redefined within each time interval according to the generator rotational speed ω_{fg}. Then, using the aforementioned technique, the energy A in the fault-related frequency band is calculated in each time interval using (7) and (8). These calculations are repeated until the whole signal has been processed. Finally, a curve of the energy variation in the fault-related frequency band is obtained, and changes in the running condition of the WT can be assessed.

This task could have been accomplished using a series of conventional bandpass filters set up to cover the expected speed range of the turbine. However, such an analysis would not have the advantages of the CWT in processing nonstationary signals shown in Fig. 1 and [18].

To verify the computational efficiency of the proposed technique compared to the traditional CWT and DWT, a calculation was performed to extract the 50-Hz energy component from 1 s of line current signal, sampled at a frequency of 2 kHz. The time taken by each approach is listed in Table I. The calculations were done in a computer with 1.4 GHz of Intel Pentium processor and 512 MB of RAM.

From Table I, it can be concluded that the proposed energy tracking technique is the most computationally efficient of the three approaches.

IV. WT CONDITION MONITORING BY POWER SIGNAL ANALYSIS

In view of the proposed advantages of generator power signal analysis for detecting both mechanical and electrical faults in a variety of designs of WT drive train, it has been applied in this paper, in combination with the energy tracking method described previously, to develop a new WT condition monitoring technique.

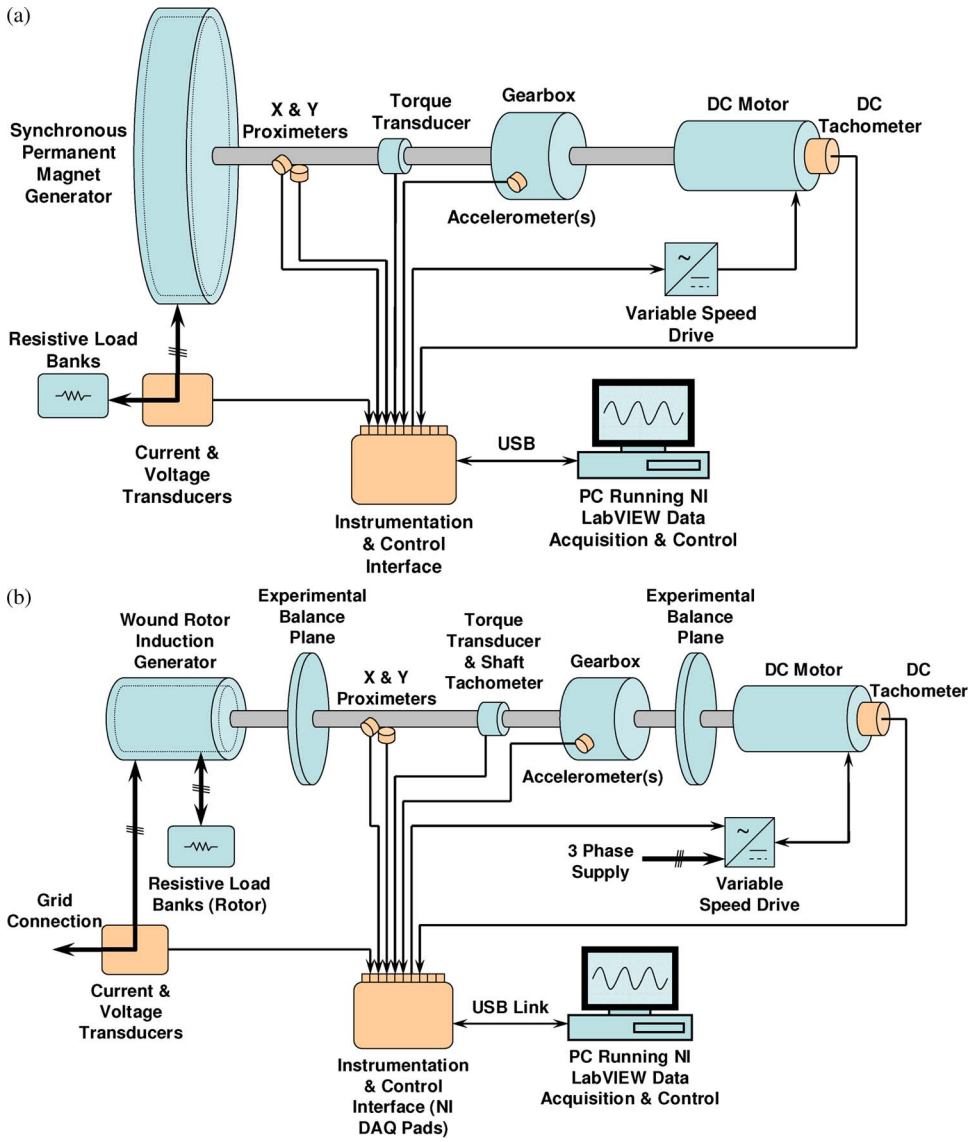

Fig. 6. Schematic diagrams of the WT drive train test rig. (a) With permanent-magnet synchronous generator installed. (b) With induction generator installed.

A. WT Drive Train Test Rig

One of the difficulties in gaining practical industry experience of condition monitoring on real WTs is the lack of collaboration needed with WT operators and manufacturers, due to data confidentiality, particularly when faults are present. This can be avoided by gaining condition monitoring experience using a controllable experimental test rig to which defined faults can be applied. Therefore, the technique proposed in this paper has been validated experimentally on a WT drive train test rig designed to investigate condition monitoring signals in the laboratory. This test rig was described in detail in [16] and was equipped first with a permanent-magnet synchronous generator and, subsequently, with an induction generator, both as shown in Fig. 6.

The synchronous generator [Fig. 6(a)], such as might be used in a direct-drive WT, was rated for the experiment at 10 kW, three-phase 54-pole permanent-magnet machine with a rectified output feeding a resistive load bank.

The induction generator [Fig. 6(b)], such as might be used in a geared-drive WT, was rated for the experiment at 30 kW, three-phase four-pole wound-rotor machine, with the rotor circuit coupled via slip rings to a three-phase resistive load bank, so that rotor electrical imbalance could be applied, and the generator stator fed the three-phase mains.

The test rig comprises a 54-kW dc variable-speed motor and a two-stage gearbox, instrumented and controlled using LabVIEW. In the experiments, a variety of wind speed inputs could be applied to the test rig via the dc motor, the speed of which is controlled by an external model incorporating the properties of natural wind at a variety of speeds and turbulences and the mechanical behavior of a 2-MW WT operating under closed-loop conditions. Relevant signals were collected from the terminals of the generator and the drive train when subjected to this driving speed.

A number of electrical and mechanical drive train faults could be applied to the test rig. Because they are not necessarily

precise replicas of WT faults, they have been called "fault-like perturbations" but contain similarities with faults on real WTs.

In this paper, to verify the efficacy of the proposed condition monitoring technique for WTs, two "faultlike perturbations" were applied to two different generator configurations as follows.

1) In the first configuration, with the synchronous generator representing a direct-drive WT, the "faultlike perturbation" applied was mechanically unbalanced on the generator rotor, representing the effect of a mechanical unbalance fault on the WT generator drive train.
2) In the second configuration, with the slip-ring induction generator representing a geared-drive WT, the "fault-like perturbation" applied was electrically asymmetric on the generator rotor, representing the effect of a rotor winding fault, brush imbalance, or air gap eccentricity in the WT generator.

Details of both experimental arrangements are described as follows.

B. Mechanical Unbalance Fault Simulated on Rotor of Synchronous Generator

The mechanical unbalance fault was simulated by attaching a 1-kg mass to the generator rotor with an equivalent rotating mass of 290.7 kg, which is ∼0.3%. This represents a balance quality grade of G 7.8 (7.8 mm/s), within the limit of G 16 (16 mm/s) prescribed in ISO1940-1:2003 for a low-speed propeller shaft, applicable to a direct-drive WT shaft. The details of this estimation are given in Appendix A. The peak-to-peak measured displacement of the generator shaft changed a little before and after the placement of the unbalanced mass, varying in the range 90–140 μm. The equivalent vibration velocity would have been 0.13–0.21 mm/s, with the generator running at the maximum rotational speed of 28 r/min well within the 0.71-mm/s limit that is acceptable for machines $\leq$ 15 kW prescribed in ISO2372:1974.

When the synchronous generator ran at varying speed representing the wind driving situation, the speed, torque, and total power were measured using a sampling frequency of 1 kHz, and the "fault-like perturbation" was periodically applied to the rotor. The time waveforms of the signals before and after the application are shown in Fig. 7(a).

From Fig. 7(a), it can be seen that, in the presence of the mass unbalance fault, the driving shaft torque signal gave a response at the shaft rotational frequency f_{rm}, as expected, fluctuating by 8% range due to the combined effects of mass unbalance fault and wind driving turbulence, which can be compared to fluctuating by 4% due to the wind driving turbulence alone. By contrast, the generator power showed only a slight change in the presence of the fault. In this case, the fault-related frequency is f_{rm}, and the CWT-based energy tracking technique was applied to extract energy at this frequency, as shown in Fig. 7(b). This provided a clear indication of the presence or absence of the mechanical unbalance fault despite the fact that the shaft speed was varying continuously throughout the experiment and the effect could not be observed in the unprocessed total power signal shown in Fig. 7(a).

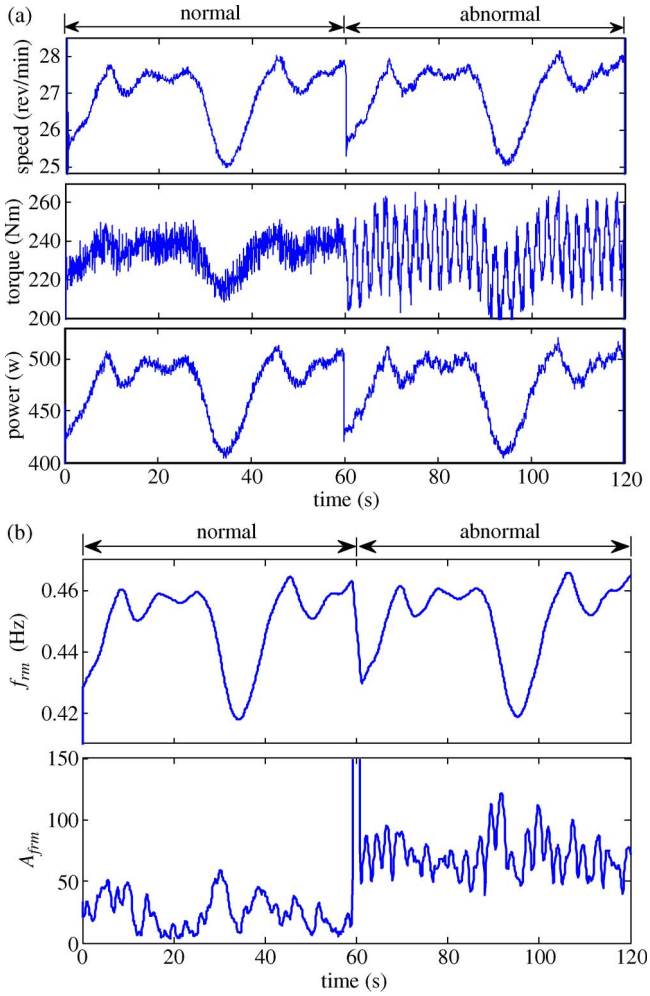

Fig. 7. Mass unbalance fault applied to a synchronous generator rotor on the WT test rig, representing a direct-drive WT. (a) Signals when a mass unbalance fault was simulated on a synchronous generator rotor. (b) Detecting a mass unbalance fault from the power signal.

TABLE II
PARAMETERS USED FOR CALCULATION RESULTS IN FIG. 7

ω_c	ω_f	T
ω_{rm}	$0.03\,\omega_{rm}$	$0.2s$

It can be seen from Fig. 7(b) that a 0.3% or G 7.8 unbalance fault was easily detectable. This shows that the proposed technique has the potential to detect an incipient mechanical unbalance fault of 0.3% or G 7.8 on a direct-drive WT. The parameters used for this calculation are given in Table II.

C. Electrical Asymmetry on Rotor of Induction Generator

The electrical asymmetry was simulated on the induction generator by adjusting the phase resistances in the load bank externally connected to the rotor. Two levels of rotor asymmetry were applied to investigate the effect of an incipient fault. These were an electrical asymmetry of $U_e = 4.7\%$ and, then, a larger asymmetry of 9.2%. The details of the rotor circuit and the estimation of asymmetry are described in Appendix B and in Table IV.

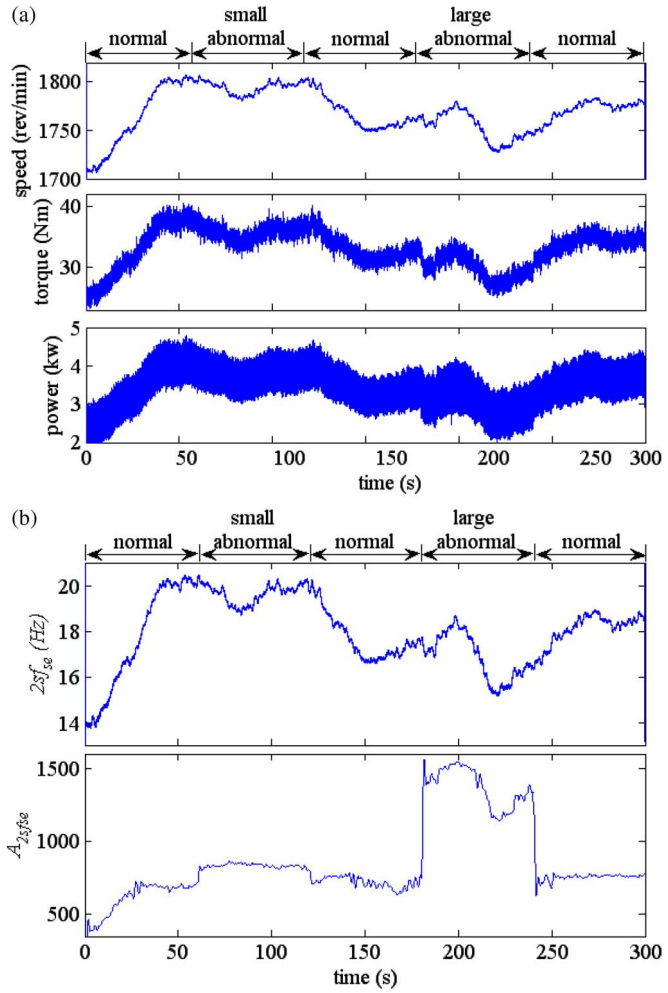

Fig. 8. Electrical asymmetry applied to an induction generator rotor on the test rig, representing a geared-drive WT. (a) Signals when an electrical asymmetry fault was simulated on an induction generator rotor. (b) Detecting an electrical asymmetry fault from the power signal.

As in the mechanical unbalance experiment, the rotational speed, mechanical drive shaft torque, and generator total power signals were measured when the "faultlike perturbation" was periodically applied to the rotor. A smaller fault was applied in the period 60–120 s and a larger fault between 180 and 240 s, with the rotor circuits being balanced in the periods 0–60 s, 120–180 s, and 240–300 s. The time waveforms of the signals collected in this experiment are shown in Fig. 8(a), and it can be seen that, due to the effect of the varying generator speed, the fault symptom cannot be observed clearly from either the generator shaft torque or total power.

When the rotor phase resistances are imbalanced, the generator current, voltage, and power are modulated twice by the slip frequency as the rotor asymmetry moves through the air gap magnetic field twice for every pole pair cycle [4]. Therefore, in this case, the fault-related frequency is $2sf_{se}$, and the CWT-based energy tracking technique was applied to extract the energy at that frequency, as shown in Fig. 8(b).

From Fig. 8(b), it can be seen that the smaller, 4.7%, fault was not clear although it is still visible, so the condition monitoring algorithm had limited detectability in this case. This lack of detectability was due to the residual imbalances present in the rotor windings, brush gear, and connections, as well as the negative influence of the timely varying generator rotational speed which partially hid the faulty feature. However, the larger 9.2% fault was clearly visible in the figure and, therefore, readily detectable despite the fact that the $2sf_{se}$ frequency signal was varying during the experimental processes.

This shows that the proposed technique has the potential to detect an incipient 9.2% electrical asymmetry fault on a geared-drive WT generator. The parameters used for this calculation are given in Table III.

TABLE III
PARAMETERS USED FOR CALCULATION RESULTS IN FIG. 8

ω_c	ω_f	T
$2sf_{se}$	$0.4sf_{se}$	$0.12s$

V. CONCLUSION

To improve the WT availability and reduce the O&M costs, a new WT condition monitoring technique has been proposed. From this research, the following conclusions can be reached.

1) In comparison with the conventional vibration, temperature measurement, and lubrication oil analysis, the technique proposed shows the following potential advantages:
   a) reduced capital cost;
   b) ability to detect both electrical and mechanical faults;
   c) applicable to both geared and direct-drive WTs.
2) The proposed CWT-based energy tracking method not only reduces the calculation needed to extract features from lengthy online data but also provides a feasible condition monitoring approach that is applicable to WTs operating at either fixed or variable speed.
3) Experiments have shown that the proposed technique is capable of detecting both mechanical and electrical faults in WT drive trains of different types.
4) The technique is a feasible way to establish a simple, cheap, but potentially global cost-effective CMS for a WT.

The technique now needs to be applied to the power signals obtained from real WTs during real mechanical and electrical faults to determine the detectability of the algorithm and its ability to detect incipient faults in both cases.

Further work will also be needed to establish the ability of this technique for a wider range of faults and for a variable-speed WT under closed-loop control.

APPENDIX A
GENERATOR ROTOR MECHANICAL UNBALANCE

Based on BS ISO1940-1:2003, the balance quality grade G may be calculated by

$$G = e \cdot 2\pi f_{rm} \tag{A1}$$

where

$$e = mr/M_{\text{eq}} \tag{A2}$$

$$U_m = (m/M_{\text{eq}}) \times 100. \tag{A3}$$

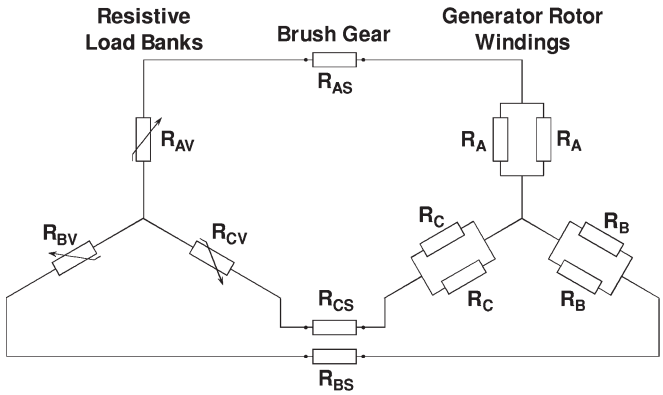

Fig. 9. Rotor circuit diagram, including a resistive load bank.

TABLE IV
ELECTRICAL ASYMMETRY APPLIED TO TEST RIG IN FIG. 8

Time (s)	Description	U_e (%)
0 – 60s	Balanced	0.0
60 – 120s	Low asymmetry	4.7
120 – 180s	Balanced	0.0
180 – 240s	High asymmetry	9.2
240 – 300s	Balanced	0.0

For the test rig shown in Fig. 6(a), the unbalance mass $m = 1.0$ kg, the effective radius $r = 865$ mm, and the equivalent rotating mass of the test rig $M_{\text{eq}} = 290.7$ kg. The average rotational speed of the generator rotor is 25 r/min. This gives a balance quality grade and mechanical unbalance for Fig. 7 of G 7.8 ($G = 7.8$ mm/s) and $U_m = 0.3\%$, respectively.

APPENDIX B
GENERATOR ROTOR ELECTRICAL ASYMMETRY

The details of the generator rotor circuit shown in Fig. 6(b) taking into account the external resistive load bank are shown in Fig. 9.

The balanced circuit resistances were given by

$$\begin{cases} R_{AB} = R_{AV} + R_{BV} + R_{AS} + R_{BS} + (R_A + R_B)/2 \\ R_{BC} = R_{BV} + R_{CV} + R_{BS} + R_{CS} + (R_B + R_C)/2 \\ R_{CA} = R_{CV} + R_{AV} + R_{CS} + R_{AS} + (R_C + R_A)/2. \end{cases} \tag{B1}$$

The circuits are balanced, giving

$$R_{AB} = R_{BC} = R_{CA} = \overline{R} = 7.60\ \Omega \tag{B2}$$

where $\overline{R} = (R_{AB} + R_{BC} + R_{CA})/3$.

Then, the electrical imbalance can be estimated through calculating the residual circuit resistance δR, i.e.,

$$\delta R = |R_{AB}e^{i\theta_1} + R_{BC}e^{i\theta_2} + R_{CA}e^{i\theta_3}| \tag{B3}$$

where $i = \sqrt{-1}$, $\theta_1 = 0$, $\theta_2 = 2\pi/3$, and $\theta_3 = 4\pi/3$.

The percentage fault can be described by

$$U_e = (\delta R/\overline{R}) \times 100. \tag{B4}$$

The larger the value of U_e, the more serious the electrical asymmetry. The electrical asymmetries applied in Fig. 8 are listed in Table IV.

ACKNOWLEDGMENT

The authors would like to thank the New and Renewable Energy Centre, Blyth, for the assistance for the original provision of the test rig.

REFERENCES

[1] J. F. Manwell, A. L. Rogers, and J. G. McGowan, "Status of offshore wind energy in the United States," in *Proc. IEEE Power Eng. Soc. Summer Meeting*, Jul. 15–19, 2001, vol. 1, pp. 10–13.
[2] H. Polinder, F. F. A. van der Pijl, G. J. de Vilder, and P. J. Tavner, "Comparison of direct-drive and geared generator concepts for wind turbines," *IEEE Trans. Energy Convers.*, vol. 21, no. 3, pp. 725–733, Sep. 2006.
[3] J. Nilsson and L. Bertling, "Maintenance management of wind power systems using condition monitoring systems—Life cycle cost analysis for two case studies," *IEEE Trans. Energy Convers.*, vol. 22, no. 1, pp. 223–229, Mar. 2007.
[4] P. J. Tavner, "Review of condition monitoring of rotating electrical machines," *IET Elect. Power Appl.*, vol. 2, no. 4, pp. 215–247, Jul. 2008.
[5] D. Casadei, F. Filippetti, A. Yazidi, C. Rossi, and G. A. Capolino, "Diagnostic technique based on rotor modulating signals signature analysis for doubly fed induction machines in wind generator systems," in *Conf. Rec. IEEE IAS Annu. Meeting*, Oct. 8–12, 2006, vol. 3, pp. 1525–1532.
[6] A. Bellini, F. Filippetti, C. Tassoni, and G. A. Capolino, "Advances in diagnostic techniques for induction machines," *IEEE Trans. Ind. Electron.*, vol. 55, no. 12, pp. 4109–4126, Dec. 2008.
[7] P. Caselitz and J. Giebhardt, "Rotor condition monitoring for improved operational safety of offshore wind energy converters," *Trans. ASME, J. Sol. Energy Eng.*, vol. 127, no. 2, pp. 253–261, May 2005.
[8] F. Spinato, P. J. Tavner, G. J. W. van Bussel, and E. Koutoulakos, "Reliability of wind turbine subassemblies," *IET Renew. Power Gener.*, vol. 3, no. 4, pp. 1–15, 2009.
[9] S. F. Legowski, A. H. M. Sadrul Ula, and A. M. Trzynadlowski, "Instantaneous power as a medium for the signature analysis of induction motors," *IEEE Trans. Ind. Appl.*, vol. 32, no. 4, pp. 904–909, Jul./Aug. 1996.
[10] W. Q. Jeffries, J. A. Chambers, and D. G. Infield, "Experience with bicoherence of electrical power for condition monitoring of wind turbine blades," *Proc. Inst. Elect. Eng.—Vis. Image Signal Process.*, vol. 145, no. 3, pp. 141–148, Jun. 1998.
[11] W. Yang, P. J. Tavner, C. J. Crabtree, and M. Wilkinson, "Research on a simple, cheap but globally effective condition monitoring technique for wind turbines," presented at the XVIII Int. Conf. Electrical Machines (ICEM), Vilamoura, Portugal, Sep. 2008, Paper ID 1053.
[12] J. Cusido, L. Romeral, J. A. Ortega, J. A. Rosero, and A. E. Garcia, "Fault detection in induction machines using power spectral density in wavelet decomposition," *IEEE Trans. Ind. Electron.*, vol. 55, no. 2, pp. 633–643, Feb. 2008.
[13] A. Ordaz-Moreno, R. de Jesus Romero-Troncoso, J. A. Vite-Frias, J. R. Rivera-Gillen, and A. Garcia-Perez, "Automatic online diagnosis algorithm for broken-bar detection on induction motors based on discrete wavelet transform for FPGA implementation," *IEEE Trans. Ind. Electron.*, vol. 55, no. 5, pp. 2193–2202, May 2008.
[14] M. Riera-Guasp, J. A. Antonino-Daviu, M. Pineda-Sanchez, R. Puche-Panadero, and J. Perez-Cruz, "A general approach for the transient detection of slip-dependent fault components based on the discrete wavelet transform," *IEEE Trans. Ind. Electron.*, vol. 55, no. 12, pp. 4167–4180, Dec. 2008.
[15] S. S. Tsai, C. T. Hsieh, and S. J. Huang, "Enhancement of damage-detection of wind turbine blades via CWT-based approaches," *IEEE Trans. Energy Convers.*, vol. 21, no. 3, pp. 776–781, Sep. 2006.
[16] W. Yang, P. J. Tavner, and M. Wilkinson, "Condition monitoring and fault diagnosis of a wind turbine synchronous generator drive train," *IET Renew. Power Gener.*, vol. 3, no. 1, pp. 1–11, Mar. 2009.
[17] E. Wiggelinkhuizen, T. Verbruggen, H. Braam, L. Rademakers, J. Xiang, and S. Watson, "Assessment of condition monitoring techniques for offshore wind farms," *Trans. ASME, J. Sol. Energy Eng.*, vol. 130, no. 3, pp. 1–9, Aug. 2008.
[18] S. K. Lee, "An acoustic decay measurement based on time–frequency analysis using wavelet transform," *J. Sound Vib.*, vol. 252, no. 1, pp. 141–153, Apr. 2002.

Wenxian Yang received the Ph.D. degree in mechanical engineering from Xi'an Jiaotong University, Xi'an, China, in 1999. He completed his postdoctoral research in Northwestern Polytechnical University, Xi'an, in 2001.

He was with the City University of Hong Kong, Kowloon, Hong Kong; Nottingham Trent University, Nottingham, U.K.; Cranfield University, Cranfield, U.K.; and Durham University, Durham, U.K. He is currently a Technical Specialist with the New and Renewable Energy Centre, Blyth, U.K. He has worked in the areas of new and renewable energy, signal processing, machine condition monitoring and fault diagnosis, nondestructive testing and nondestructive evaluation, and artificial intelligence in both industry and academia.

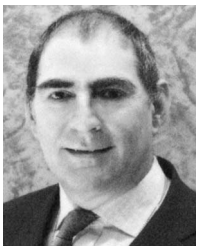

Peter J. Tavner (SM'08) received the M.A. degree from Cambridge University, Cambridge, U.K., in 1969 and the Ph.D. degree from Southampton University, Southampton, U.K., in 1978.

He held research and technical positions in the industry, including being a Group Technical Director with FKI Energy Technology, Loughborough, U.K. He is currently a Professor of new and renewable energy and the Head of the School of Engineering and Computing Sciences, Durham University, Durham, U.K. His research interest includes machines for renewable energy, condition monitoring, and reliability.

Dr. Tavner was the recipient of the Institution Premium of the Institution of Electrical Engineers, U.K.

Christopher J. Crabtree received the M.Eng. degree in engineering from Durham University, Durham, U.K., in 2007, having studied new and renewable energy as an electrical engineer, where he is currently working toward the Ph.D. degree in condition monitoring of offshore wind turbines.

His research interests include the development of condition monitoring techniques using industrial data and a test rig.

Michael Wilkinson received the M.Sc. degree in electromagnetic sensing from Durham University, Durham, U.K., in 2003 and the Eng.D. degree with a thesis on condition monitoring for offshore wind turbines from Newcastle University, Newcastle upon Tyne, U.K., in 2007, in a collaborative project with Durham University and FKI Energy Technology.

In 2007, he joined Garrad Hassan, Bristol, U.K., as part of the operational projects team, where he has been monitoring wind farms worldwide on behalf of owners. His research interests include condition monitoring and reliability of wind turbines.